Results in Physics 13 (2019) 102319

Contents lists available at ScienceDirect

Results in Physics

journal homepage: www.elsevier.com/locate/rinp

Mechanical properties and corrosion behavior of copper based hybrid composites synthesized by stir casting

Manvandra Kumar Singh[a], Rakesh Kumar Gautam[b], Gopal Ji[c,*]

[a] Department of Mechanical Engineering, Mewar University-Chittorgarh, Rajasthan 312901, India
[b] Department of Mechanical Engineering, Indian Institute of Technology (BHU) Varanasi, Uttar Pradesh 221005, India
[c] School of Materials Science and Technology, Indian Institute of Technology (BHU) Varanasi, Uttar Pradesh 221005, India

ARTICLE INFO

Keywords:
Copper
Corrosion
Hybrid composite
Hardness
Impedance
Stir casting

ABSTRACT

In this work, we are reporting development of copper – highly strained stainless steel (HSSS) – tungsten carbide (WC) hybrid composites as well as their mechanical behavior and corrosion resistant properties (0.1 M NaCl). Three types of Cu-HSSS-WC hybrid composites, having different quantity of HSSS (A1-1%, A2-2% and A4-4%), are prepared by stir casting and shaped in strip form. These strips are characterized by X-ray diffraction, scanning electron microscopy and energy dispersive X-ray analysis techniques along with micro-structure analysis. The corrosion resistances of the composites are determined by alternating current impedance measurements and Tafel polarization curves. The electrochemical results portray that composites can be arranged as per their corrosion resistance as: A4 > A2 > A1; which is same order of the composites as reported by hardness and ultimate tensile strength values. The results show that the prepared composites have greater hardness, ultimate tensile strength and corrosion resistance in comparison to bare copper.

Introduction

Copper based composites are extensively used in electronic and automotive industries due to their excellent wear resistance, corrosion resistance, mechanical properties and electrical properties [1–4]. As reinforcement materials, the ceramics are substantially used in the development of copper matrix composites for their pronounced wear resistance, corrosion resistance, hardness and cost effectiveness [5,6]. However, copper is reported to have inferior wetting characteristics for the ceramics, which promotes poor bonding between copper matrix and ceramics reinforcement [7,8]. Due to this, the mechanical properties of the composites suffer because the transfer of force from copper to strong ceramic particles is impeded.

As per the investigation reports, copper based composites show better mechanical properties with stainless steel reinforcements than ceramic reinforcements [9–11]. This occurs due to greater wettability of copper for metals than ceramics. The poor wettability of copper for ceramics and superior wettability for stainless steels have motivated the necessity of developing copper-stainless steel-ceramics hybrid composites. Thus prepared copper matrix composites can have simultaneous advantage of ceramics and stainless steel reinforcement. The concept of hybrid composite is to reinforce the matrix either with more than one material or with single material in two different physical forms (particulate and fiber) [12]. Till now, many hybrid composites have been developed for different applications [13–17]. However, the hybrid composites developed in this work have not been reported till date. Taking inspiration from this thought, the copper-HSSS-WC hybrid composites are developed by stir casting in this work. WC is a high strength material having high wear resistance, hot hardness, deformation resistance, rigidity and impact resistance. The HSSS used in this work is in fact chips and particles produced during machining of stainless steels. The steel chips and particles are the problems of industries in many countries as they have no concrete plan for the effective reuse of them. Thus, they are an industrial waste. In addition, these chips and particles are highly strained and possess greater strength than bulk steel due to refined microstructure. Hence, both chips and particles of HSSS are selected as reinforcement along with WC in copper matrix.

The main aim of present work is to develop Cu-HSSS-WC composites by stir casting and to investigate their mechanical properties and corrosion behavior. In this work, three different concentrations of HSSS are used in the development of Cu-HSSS-WC hybrid composites. This is done to highlight the effect of HSSS addition on the mechanical and corrosion resistant properties of the composites. Accordingly, they have been assigned different codes: Cu-1% HSSS-WC, A1; Cu-2%HSSS-WC, A2; and Cu-4%HSSS-WC, A4.

* Corresponding author.
E-mail addresses: mksingh.rs.mec13@itbhu.ac.in (M.K. Singh), gopalji.rs.mst11@itbhu.ac.in (G. Ji).

https://doi.org/10.1016/j.rinp.2019.102319
Received 6 January 2019; Received in revised form 27 April 2019; Accepted 27 April 2019
Available online 09 May 2019
2211-3797/ © 2019 Published by Elsevier B.V. This is an open access article under the CC BY-NC-ND license (http://creativecommons.org/licenses/BY-NC-ND/4.0/).

Table 1
Compositional details of the materials developed by stir casting.

Materials	Compositions	Wt (%)	Wt (g)
Cu	Cu	100	1000
A1	Cu	96	960
	HSSS	1	10
	WC	1	10
	Cr	2	20
A2	Cu	95	950
	HSSS	2	20
	WC	1	10
	Cr	2	20
A4	Cu	93	930
	HSSS	4	40
	WC	1	10
	Cr	2	20

Materials and experimental details

The matrix material (Cu, 99.5% purity) was obtained from the local suppliers in Varanasi. The other materials used in development of hybrid composites, i.e., tungsten carbide (WC) and chromium (Cr) particles, were purchased from Sigma Aldrich (USA). Cr (2%-wt) is added during preparation of all the composites for better fluidity of the molten metal. HSSS is added in the form of both chips and particles and produced during machining of stainless steels. Due to irregular geometry and dimension of HSSS particles, sieving was performed and the particles having size below 80–90 μm were used along with chips in the hybrid composites.

The compositional details of the materials used in development of Cu-HSSS-WC hybrid composites are given in Table 1. For development of hybrid composite A1, the calculated amount of copper (rod) was cut into small pieces and kept in the graphite crucible. The crucible was put in the electric muffle furnace and temperature was set to 1200 °C. As soon as the temperature reached to 1200 °C, the weighed WC and Cr particles as well as HSSS particles and chips were poured into the molten copper metal. During this process, graphite stirrer was employed to stir the molten materials for 15 min at 500 RPM. Afterwards, the molten materials were poured into the permanent steel mould and air cooled for 3 hr to bring it to room temperature. Other hybrid composites, i.e., A2 and A4, were prepared by the same process.

The morphological as well as compositional details of the reinforcing materials and hybrid composites were obtained by scanning electron microscope (SEM) of Carl ZEISS (model no.-EVO/18, Germany), coupled with X-ACT detector of Oxford instruments. The crystallographic information of the hybrid composites was obtained by mini-Flex 600, Rigaku (Japan) X-ray instrument coupled with DTEX-ultra detector. The X-ray diffraction (XRD) characterization was done in the 2θ angle range of 20° − 100°.

The microstructures of the developed composites were analyzed by optical microscope of De-winter Optical Inc (India). For this analysis, the test samples were prepared in a particular manner. First, the samples were grinded with the emery papers of 400, 800, 1200 and 1600 grit size, sequentially. Then, fine polishing of the samples was done with velvet cloths having evenly distributed tufted fabric and short dense pile fibers. The etchant, i.e., 10 g $FeCl_3$ + 10 mL HCl + 100 mL distilled water, was applied to the materials under investigation (Cu, A1, A2 and A4) and left for 10 s before taking images by optical microscope. The hardness of the developed composites as well as copper was measured by the Vickers hardness tester under the normal load of 100 g for dwell time of 10 s.

The electrochemical tests were performed on the samples (area-1 cm^2) after 1 h immersion in 0.1 M NaCl at room temperature (25 ± 2 °C). The tests were operationally controlled by SP-200, bio-logic potentiostat. Three electrodes were used in the test: reference electrode, Metrohm Ag/AgCl tubular electrode; counter electrode, Metrohm platinum tubular electrode; and working electrodes, the test samples (Cu, A1, A2 and A4). For impedance measurements, the test samples were examined in the range of 10,000 Hz to 0.01 Hz with 5 mV a.c. signal. The polarization curves were obtained by examining the test samples in the potential range of OCP ± 250 mV (vs reference electrode) at a scan rate of 30 mV per minute. The voltage was swiped from cathodic potential to anodic potential. The data of polarization curves was extrapolated to obtain different parameters like corrosion current density (I_{corr}) and equilibrium corrosion potentials (E_{corr}). The impedance data was fit by ZSim (version-3.22) and different parameters related to corrosion was obtained.

The corrosion behavior of the developed hybrid composites have been probed in 0.1 M NaCl by electrochemical impedance spectroscopy (EIS) and Tafel polarization curves (TPC). The mechanical properties are investigated by Vickers hardness measurement, tensile testing and fractography analysis. The results are compared with the bare copper, which portray that the hybrid composites have much higher corrosion resistance and improved mechanical properties.

Results and discussion

Fig. 1 shows the morphology of HSSS and WC, which are used as reinforcement in the copper matrix. It was evident form Fig. 1a that HSSS was in the form of strained chips and spherical particles, which matched with the description of HSSS provided in the experimental

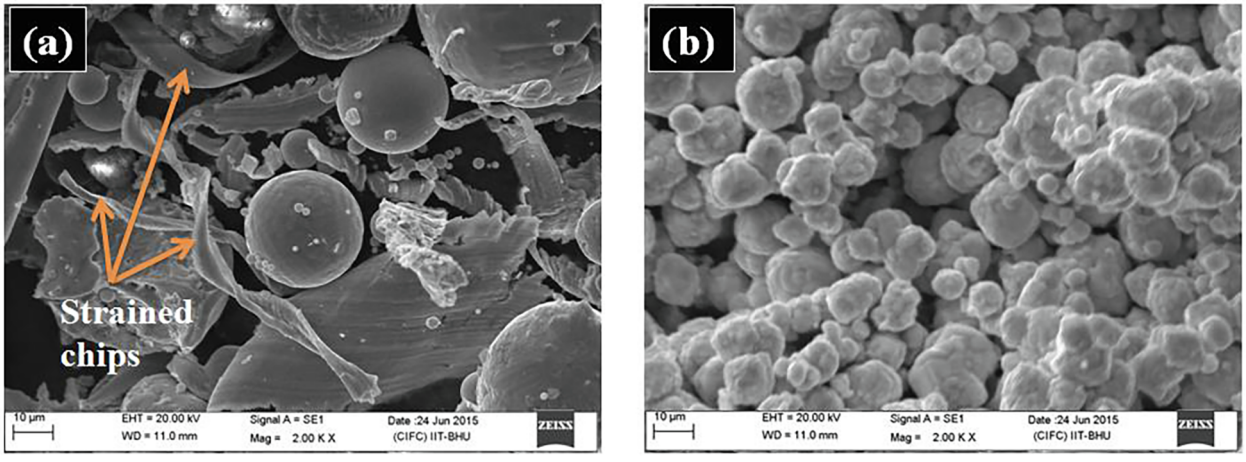

Fig. 1. SEM images of reinforcing materials (a) HSSS and (b) WC.

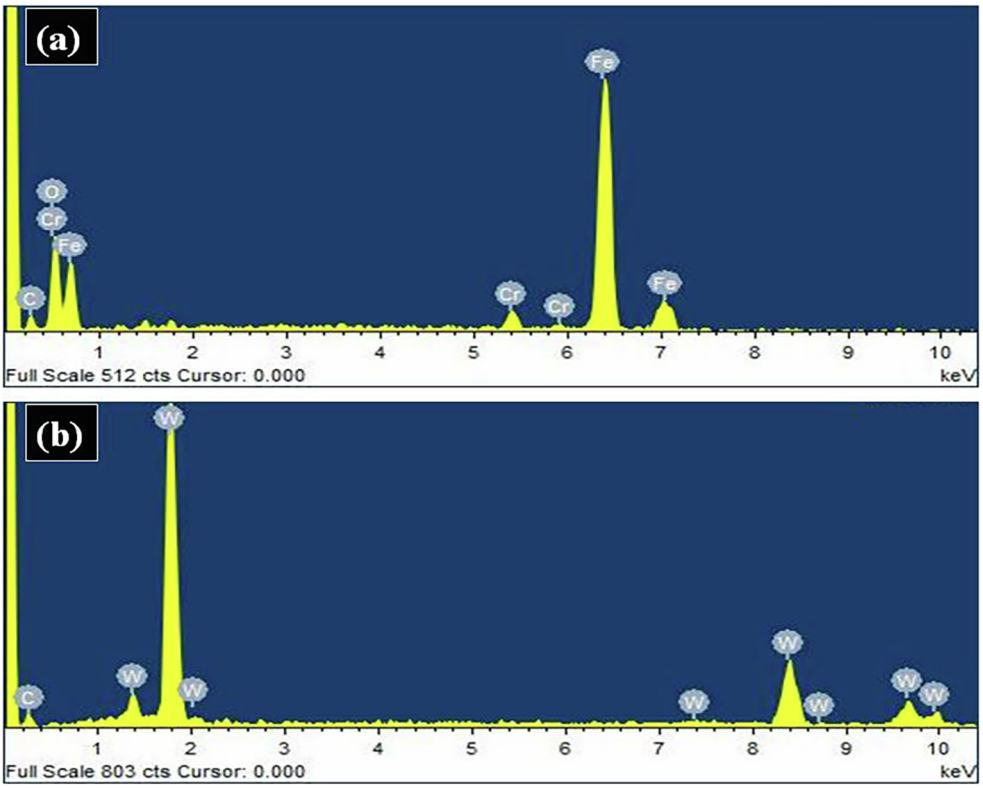

Fig. 2. EDAX spectra of reinforcing materials (a) HSSS and (b) WC.

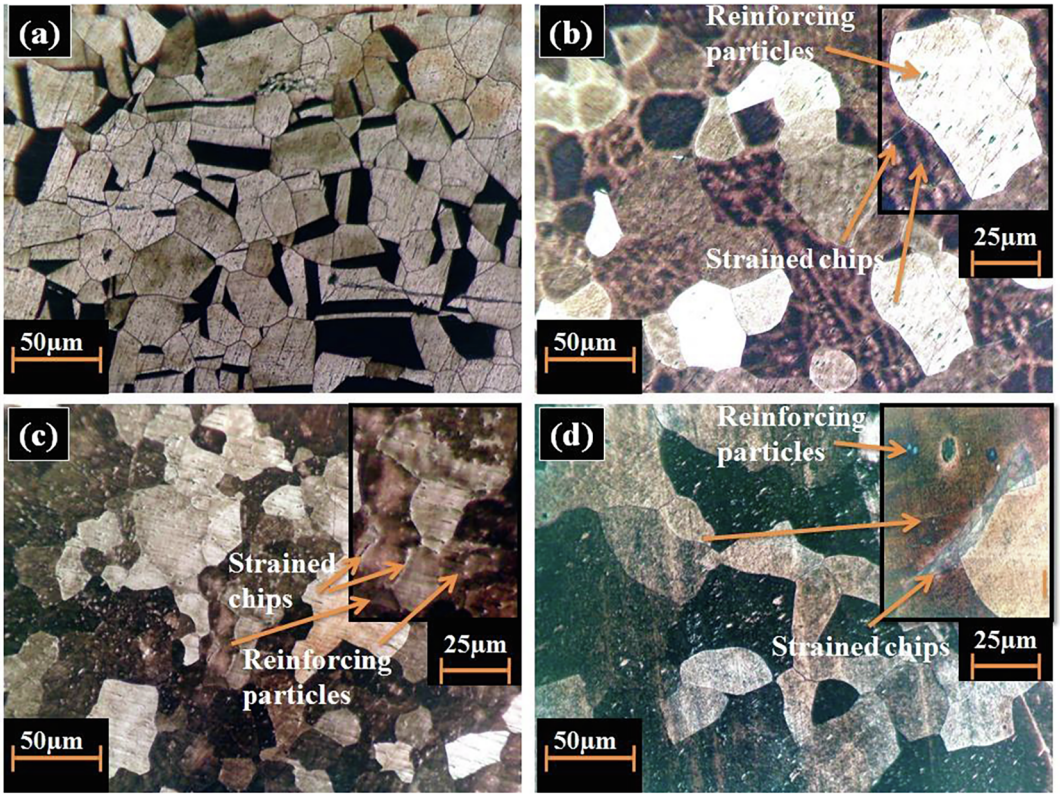

Fig. 3. Microstructures of cast (a) Cu, (b) A1, (c) A2 and (d) A4.

details. Fig. 1b revealed that the WC particles were in the spherical shape and similar in size, which could yield the uniform distribution of WC particles in the copper matrix. Furthermore, EDAX analysis was performed on the whole region of Fig. 1a and b for compositional details of WC and HSSS. The results are presented in Fig. 2. The EDAX spectrum of HSSS confirmed the presence of major elements, viz., carbon, chromium and iron. The compositional details of the HSSS was (wt%): C, 10.57; Cr, 3.46; Fe, 80.48 and O, 5.49. The presence of oxygen could be attributed to the oxidation of stainless steel due to high temperature generation during machining. Fig. 2b portrayed that WC particles were having composition (wt%): C-26.83 and W-73.17. Thus, the characterization of reinforcement materials confirmed their geometry and composition, which was necessary before proceeding further with high reliability.

Characterization of cast copper and the hybrid composites

Microstructures

The microstructures of cast copper and hybrid composites are presented in Fig. 3. The microstructures revealed that there were significant changes in the copper matrix due to reinforcement. Fig. 3b showed presence of reinforcing particles as well as strained chips in the copper matrix; however, the presence of reinforcement was clearer at higher magnification. This might be due to low concentration of reinforcement (HSSS). In contrast, presence of reinforcement material could be clearly seen for A2 and A4. Overall analysis of Fig. 3 informed that there were changes in grains alignment in the copper matrix due to reinforcing particles and strain chips in the hybrid composites. However, we could not differentiate between WC reinforcing particles and HSSS reinforcing particles in microstructure analysis due to close dimensions of the WC and HSSS particles.

EDAX mappings

The analysis of cast copper and hybrid composites was also performed by EDAX mappings. The results are presented in Figs. 4–8. The images portrayed that surface morphology of the hybrid composites were clearly different from copper, which confirmed that the structural changes occurred in copper matrix due to reinforcement. EDAX mappings of the composites projected that different elements, viz., O, C, Fe, Cr and W, were present in the copper matrix, which confirmed the formation of hybrid composites. The mappings also revealed that distribution density of Fe in copper matrix was different in A1, A2 and A4, which could correspond to different concentration of HSSS in hybrid composites. To achieve more details on the changes, EDAX spectrum analysis was performed on the same area as used in EDAX mapping. The spectra for copper and hybrid composites are shown in Fig. 8. As per EDAX analysis, the compositional details of the cast copper, A1, A2 and A4 is provided in Table 2. The elemental details of the hybrid composites revealed that reinforcement materials, viz., WC (W and C) and HSSS (Fe) were present in the copper matrix, which matched with the information provided by EDAX mapping.

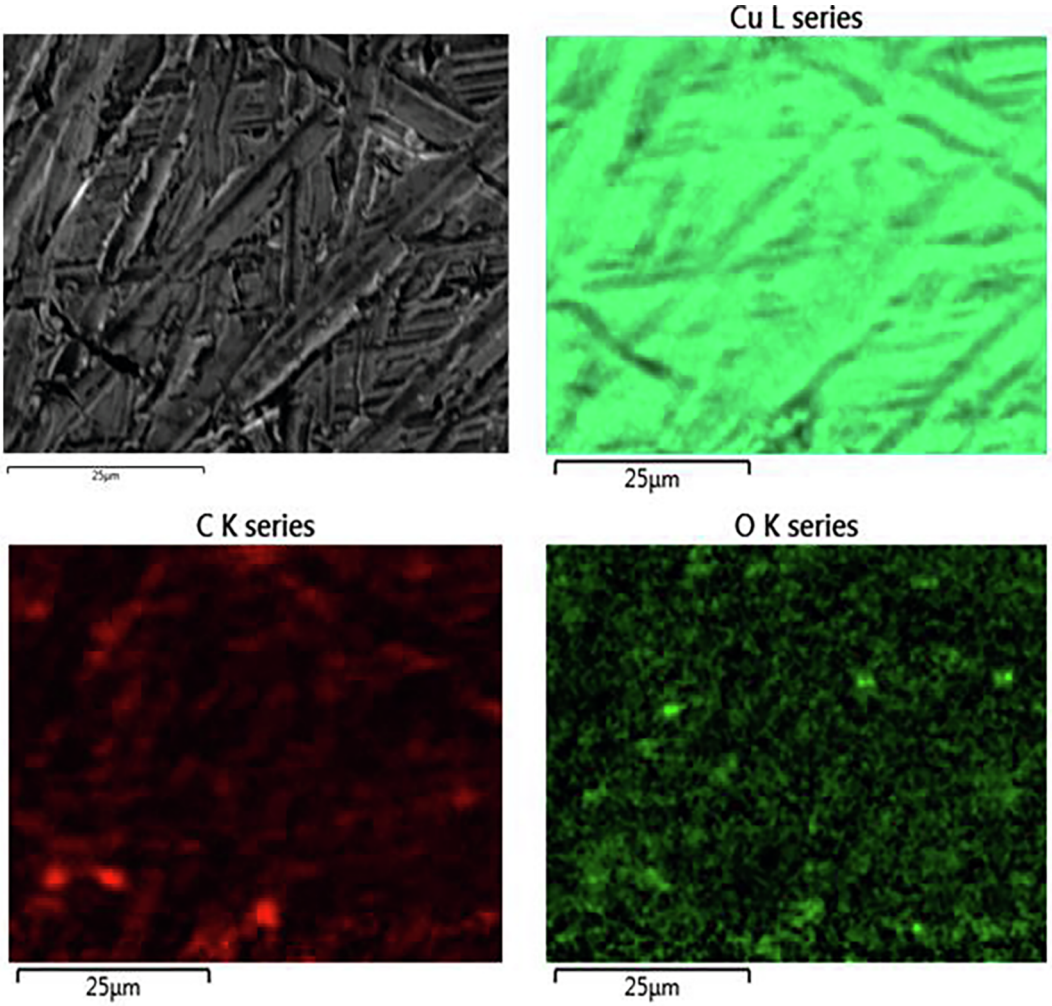

Fig. 4. SEM image and corresponding EDAX mapping of cast Cu.

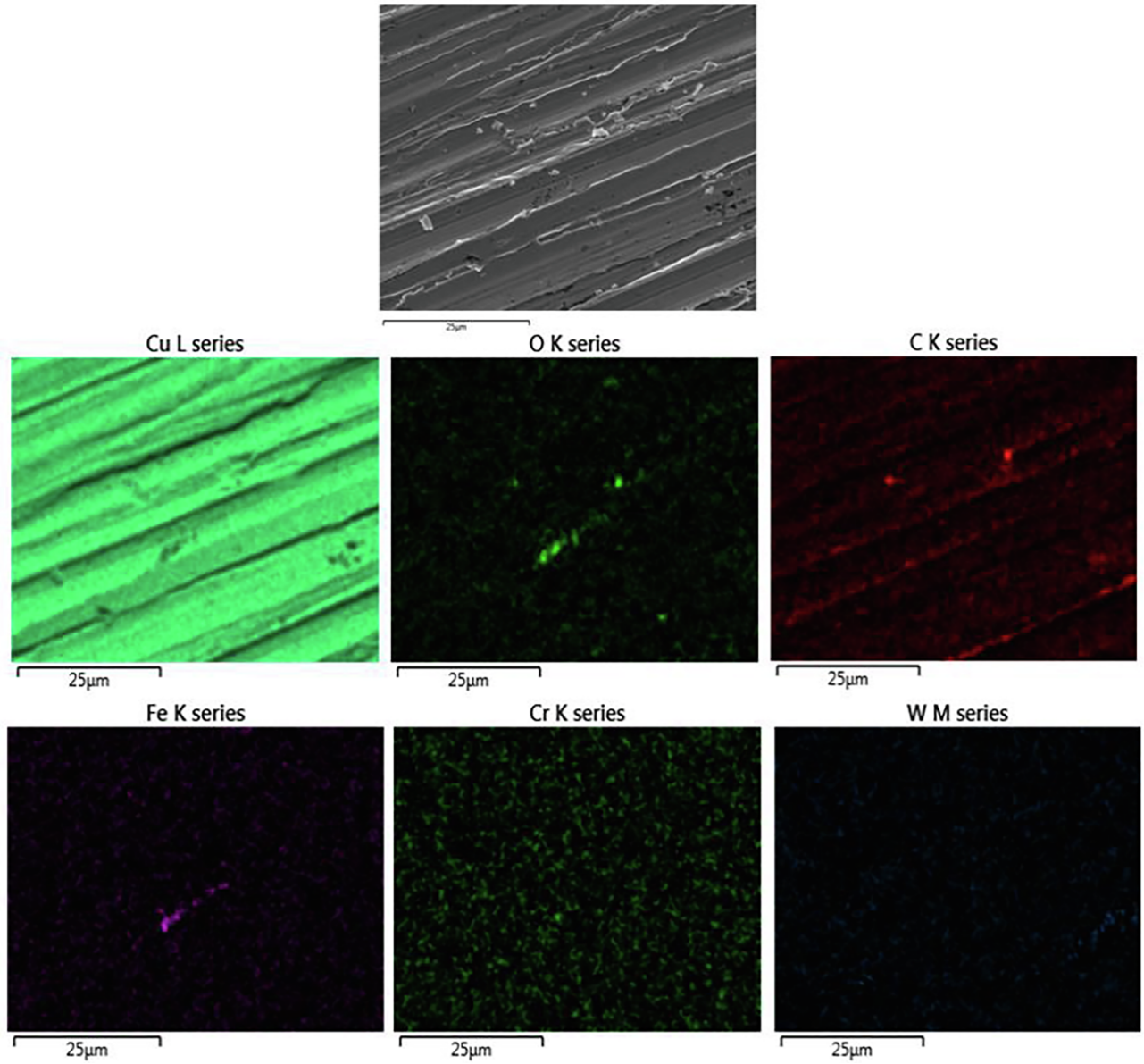

Fig. 5. SEM image and corresponding EDAX mapping of cast A1.

XRD patterns

Fig. 9 presents the XRD patterns of cast copper and hybrid composites. It was noticed that all peaks of copper were appeared in the XRD patterns of A1, A2 and A4; whereas no new peaks were detected in the XRD patterns of the hybrid composites. This fact could portray that no new phases were formed due to either interaction of reinforcing materials with the copper matrix or interaction between reinforcing materials. Another reason for absence of new peaks in XRD patterns of the composites could be the low amount (< 5%) of reinforcement materials [18,19]. However, a careful inspection of Fig. 9 revealed that the peak intensities and peaks width of the composites were changed in reference to cast copper, showing effect of reinforcement. For further investigation of this information, the XRD peaks were assigned to different planes with the help of JCPDS data (PCPDFWIN-PDF#040836). Also, full width at half maxima (FWHM) value of XRD peaks were calculated for cast copper, A1, A2 and A4 (listed in Table 3). Analysis of the data suggested that the FWHM of the peaks in A1, A2 and A4 were different from copper, which indicated the difference of crystallite size and internal strain in copper and hybrid composites [19,20]. Hence, it could be stated based on XRD patterns analysis that reinforcement materials had an effect on crystalline behavior of copper matrix and grain size.

Mechanical properties of cast copper and hybrid composites

Fig. 10 presents the hardness values of cast copper and hybrid composites. Analysis of Fig. 10 revealed that the composites exhibited greater hardness than copper. This fact could portray that the porosity of the hybrid composites went down with the addition of HSSS and WC in copper matrix [21], which could be the result of improved wettability of copper matrix for reinforcement materials. The order of hardness can be given as: A4 > A2 > A1 > Cu; which suggested that hardness of the composites increased with the weight percentage of the HSSS in the copper matrix.

The tensile properties of copper and composites are shown in Fig. 11. The ultimate tensile strength (UTS) of the materials could be ranked as per their values as: A4 > A2 > A1 > Cu. The increased UTS of the hybrid composites could be the result of strong bonding

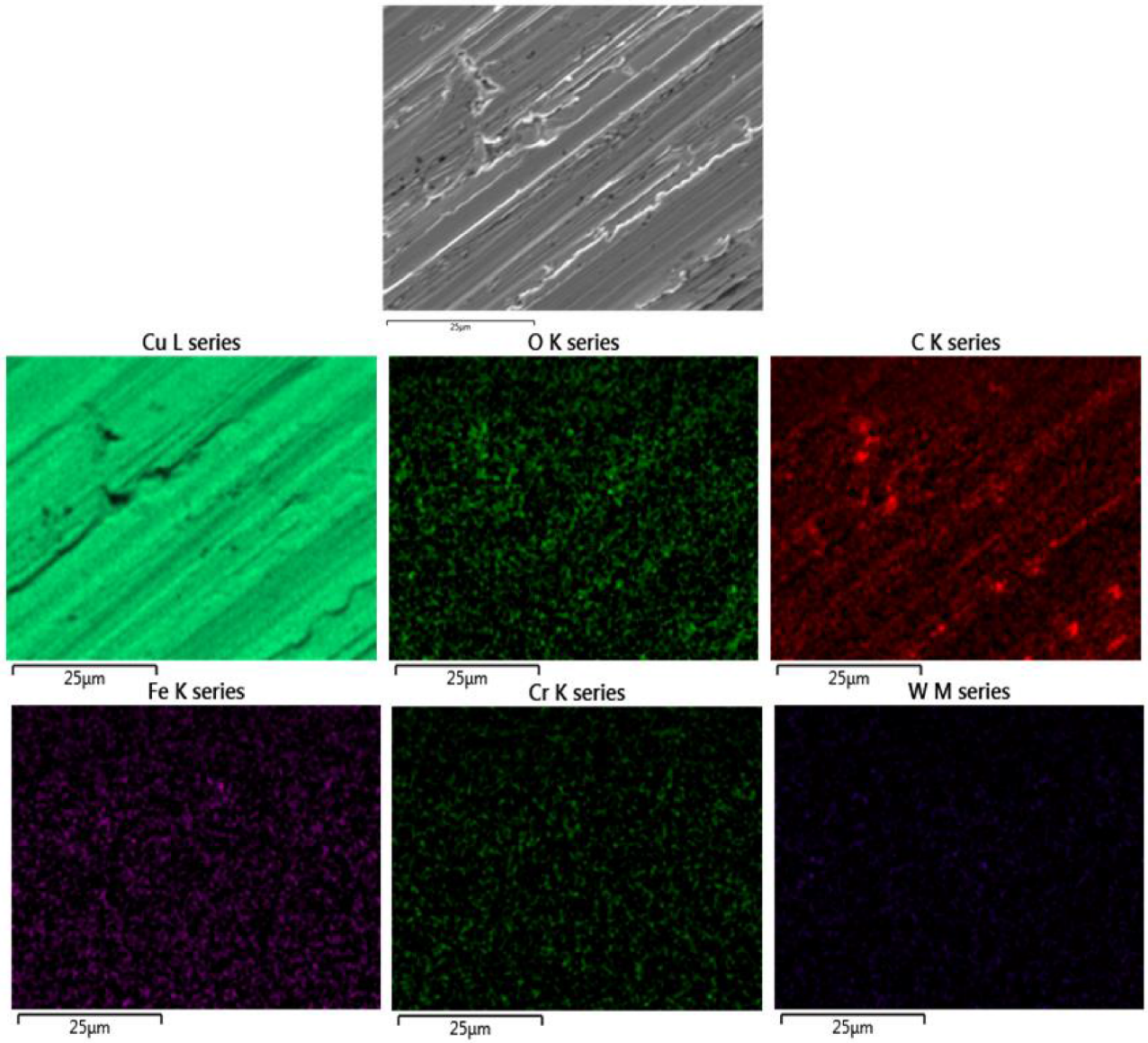

Fig. 6. SEM image and corresponding EDAX mapping of cast A2.

between reinforcement materials and copper matrix, which retarded the movement of dislocations across reinforcement-matrix interface in more successful manner in composites than in cast copper [21]. The increase in UTS could also happen due to effective transfer of load from relatively soft copper matrix to hard materials (WC and HSSS) [22]. In contrast, ductility of the developed composites was reduced, which could be attributed to addition of harder reinforcement materials (WC and HSSS) in the copper matrix.

To explain the role of WC and HSSS reinforcement in increase of hardness and UTS of the composites, fractography analysis of the surfaces was performed. Fig. 12 presents SEM images of the fractured surfaces. The preliminary analysis of the fractographs of pure copper and hybrid composites revealed that cast copper was having greater number of pores, which confirmed that hardness of the composites could increase due to reduction in porosity of the structure. Fractograph of the cast copper also revealed that there were large spherical dimples on the fractured surface. Presence of numerous large spherical dimples indicated that fracture was ductile and could appear as a result of micro voids enlargement due to uniaxial tensile stress. In the fractographs of the composites, presence of parabolic dimples as well as small spherical dimples portrayed that this fracture was ductile also. However, the shape of dimples changed from large spheres to small spheres/parabolic spheres, which could indicate that the fracture occurred due to shear force. Further analysis of the fractographs of A1, A2 and A4 revealed that undistorted reinforcement particles were embedded in the cavity of the matrix. This could suggest that reinforcement materials (WC particles, HSSS particles and chips) averted the crack propagation in the matrix and provided additional strength to the copper. The reinforcement particles did not look fractured as revealed by the fractographs of the composites, which meant that shear stress at matrix-reinforcement interface did not cross the fracture limit of the reinforcements. Thus, it could be stated based on fractograph results that WC and HSSS reinforcements were present in the copper matrix and provided additional strength to matrix against fracture. Due to this, hardness and UTS of the composites were increased.

Corrosion behavior

Corrosion behaviors of cast copper and hybrid composites have been examined by EIS and Tafel polarization curves. Fig. 13 presents

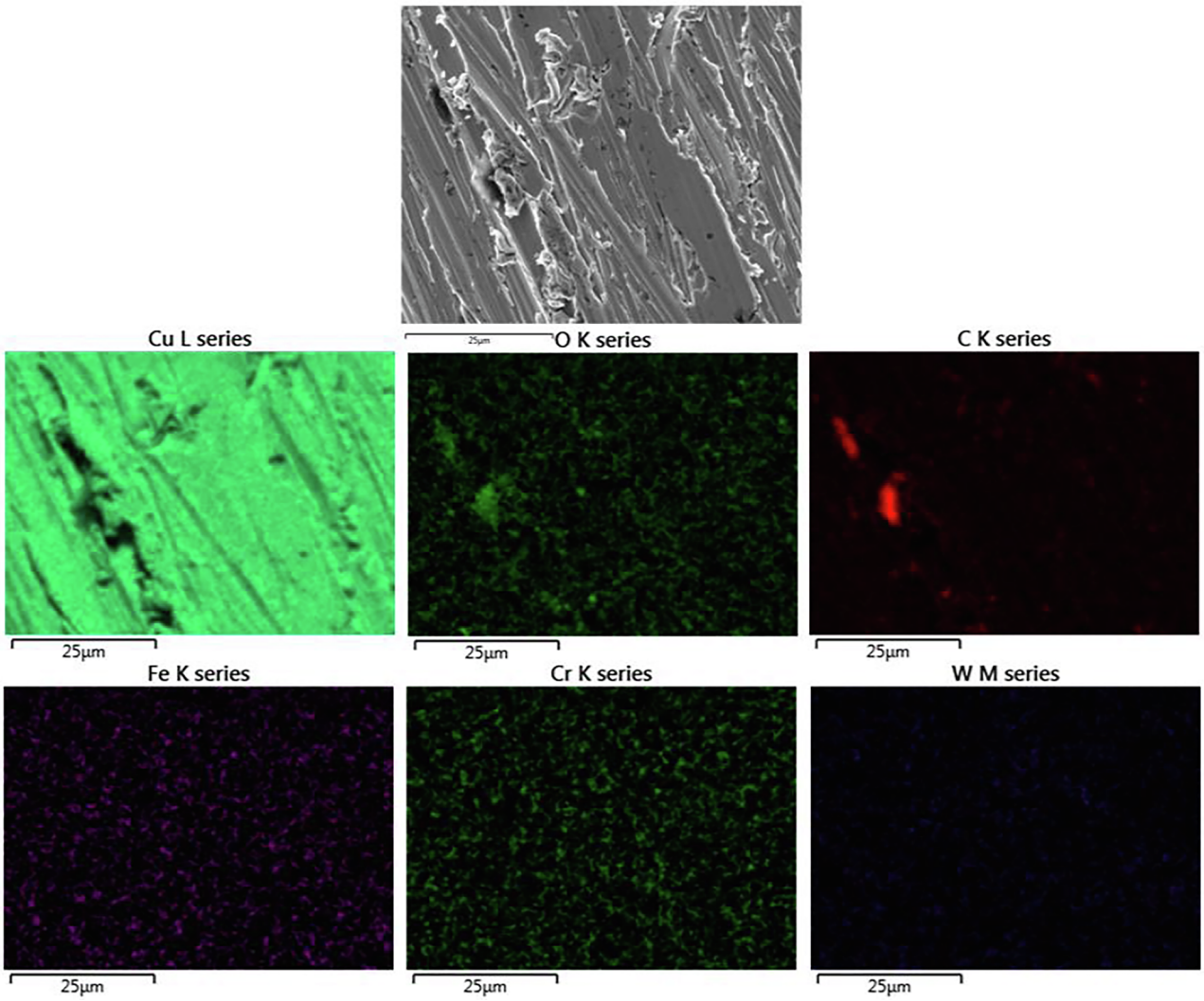

Fig. 7. SEM image and corresponding EDAX mapping of cast A4.

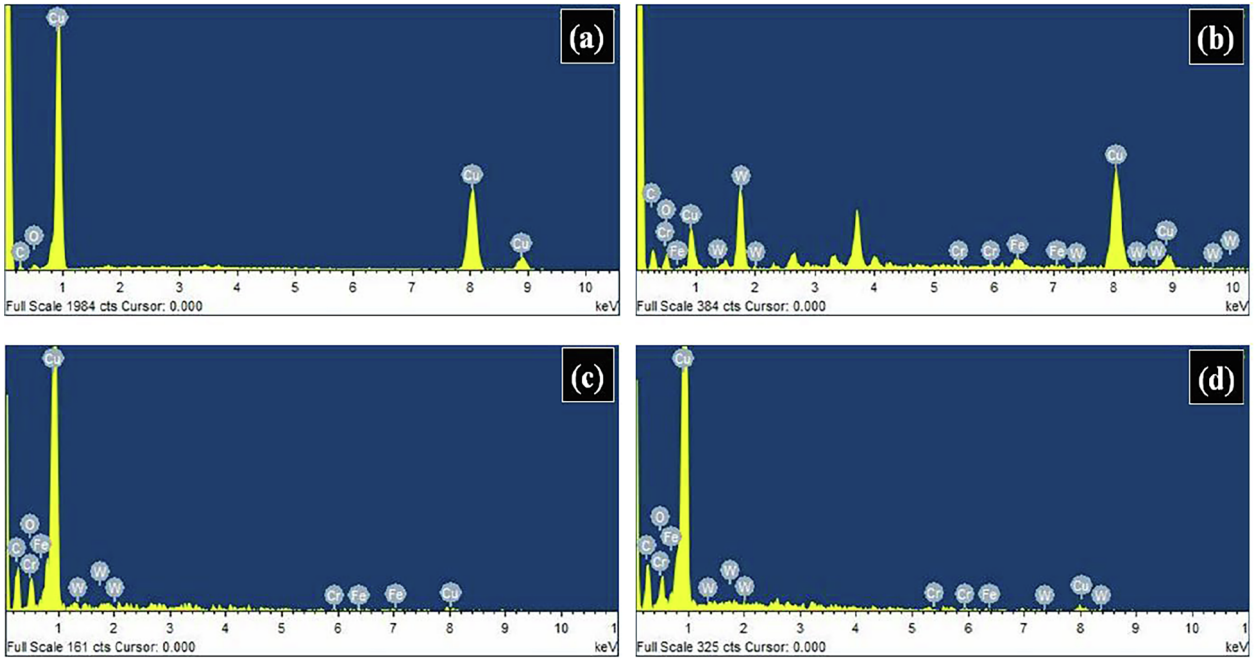

Fig. 8. EDAX spectra of cast (a) Cu, (b) A1, (c) A2 and (d) A4.

Table 2
The compositional details of cast copper and hybrid composites obtained by EDAX analysis.

Materials	Elements (weight %)					
	Cu	C	O	Cr	W	Fe
Cu	91.67	5.53	2.80	–	–	–
A1	73.47	12.90	3.82	1.20	6.52	2.09
A2	72.12	13.93	3.81	4.42	1.36	4.36
A4	73.14	13.35	2.54	4.68	1.48	4.81

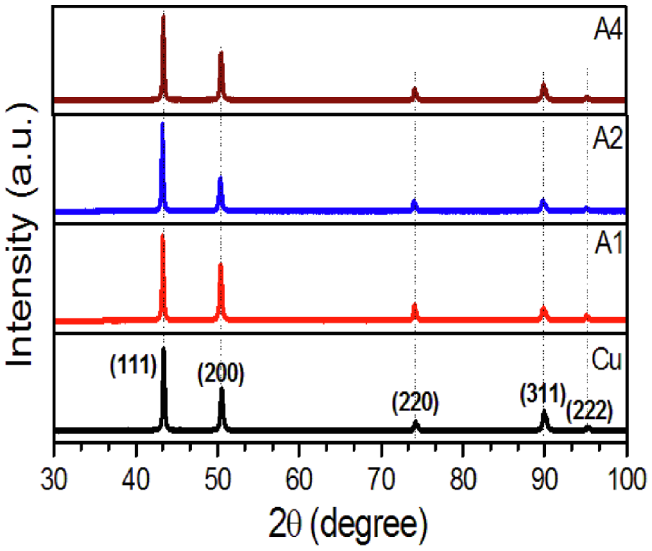

Fig. 9. XRD patterns of cast Cu, A1, A2 and A4.

Table 3
Details of peak position, diffraction planes and FWHM of XRD peaks in cast Cu, A1, A2 and A4.

Peak Position	Planes	FWHM (°2θ) of copper	FWHM (°2θ) of A1	FWHM (°2θ) of A2	FWHM (°2θ) of A4
43.38	(1 1 1)	0.1489	0.1501	0.1539	0.2288
50.44	(2 0 0)	0.2313	0.2487	0.2509	0.2931
74.12	(2 2 0)	0.1714	0.3005	0.3167	0.3879
89.84	(3 1 1)	0.2920	0.3136	0.3893	0.5234
95.09	(2 2 2)	0.2026	0.2283	0.2642	0.3918

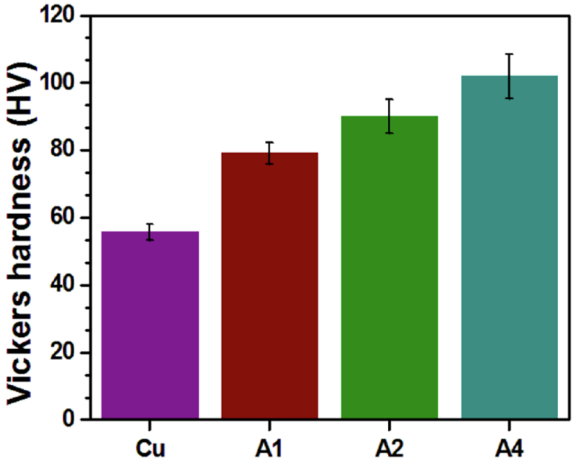

Fig. 10. Vicker's hardness measurements of cast Cu, A1, A2 and A4.

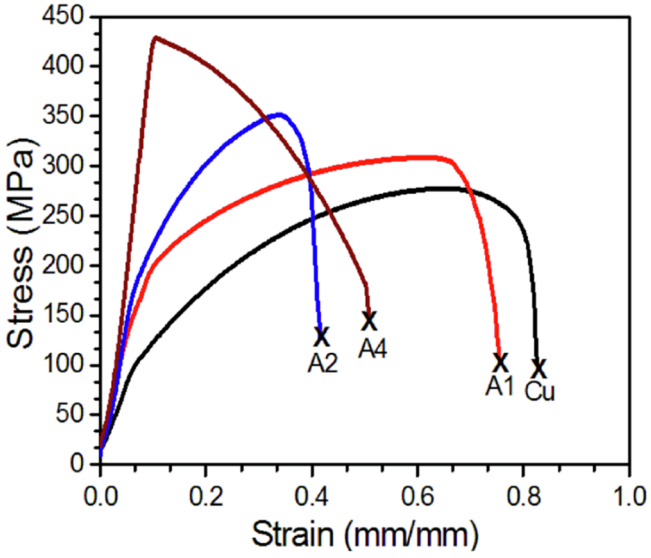

Fig. 11. Stress–strain curves of cast Cu, A1, A2 and A4.

the impedance responses of the electrodes in 0.1 M NaCl and introduces an analogous electrical circuit (AEC) for fitting of the impedance curves. Nyquist plots of both Cu and composites were constituted with a capacitive loop in high frequency zone and an inclined line in low frequency zone. The capacitive loop could be linked with the charge transfer reactions at electrode–electrolyte interface; whereas inclined line could correspond to transportation of either chloride ions or formed complexes during corrosion [23,24]. The corrosion resistance of a metal electrode is usually determined with the diameter of capacitive loop. This fact suggested that corrosion resistance of the copper and composites could be arranged as: A4 > A2 > A1 > Cu; which portrayed that HSSS concentration directly affected the corrosion properties of the composites. In presence of HSSS in composites, the corrosion attack of sodium chloride was impeded more effectively than in case of cast copper. This comment could be well supported by bode phase angle plots. Fig. 13b depicted that phase angle for hybrid composites were higher than copper, which was an indication of lesser corrosion damage in copper based hybrid composites than alone copper [25,26].

As per primary information obtained from Nyquist plots and bode phase angle plots, it was revealed that there was only one interface between electrolyte and electrodes. To confirm this preliminary information, the Nyquist plots are fitted with AEC shown in Fig. 13a. The various elements of AEC, such as, electrolyte resistance (R_s), charge transfer resistance (R_{ct}) and constant phase element (CPE) are calculated by fitting and listed in Table 4. W in the circuit is Warburg coefficient and used to consider diffusion of chloride ions towards the electrode and (or) metal-chloride complexes to the solution [27,28]. W can be used for comparative study as W is inversely proportional to Warburg impedance.

Analysis of Table 4 portrayed that R_{ct} of the electrodes amplified with the HSSS concentration in the hybrid composites. The rise in R_{ct} was 1.7 times, 2.4 times and 3.1 times of cast copper in A1, A2 and A4.

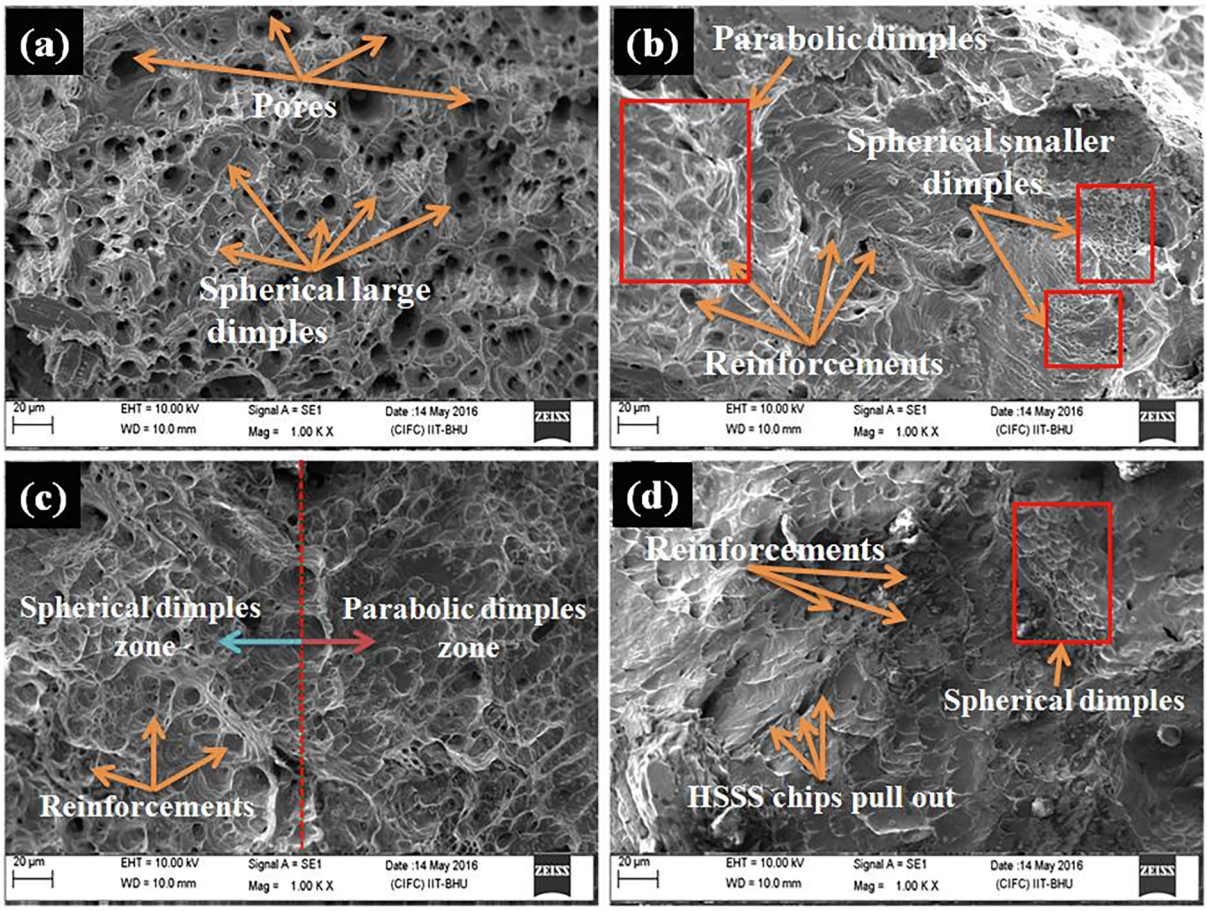

Fig. 12. SEM images of the fractured surfaces of (a) Cu, (b) A1, (c) A2 and (d) A4.

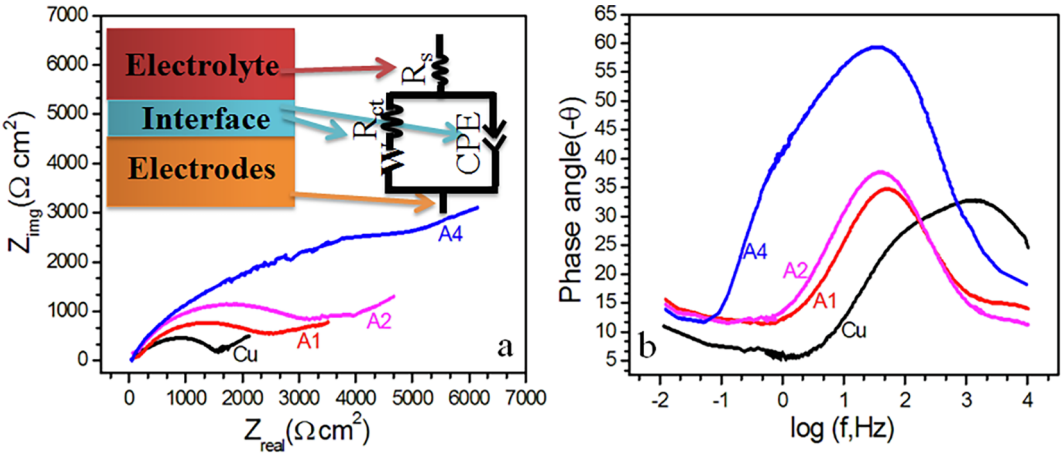

Fig. 13. Impedance response of Cu, A1, A2 and A4 in 0.1 M NaCl in form of (a) Nyquist plots and (b) bode phase angle plots.

This significant increase showed that redox activities at the surface of A1/A2/A4 were reduced, which resulted in less dissolution of metal and/or reduction of active species at the surface. As R_{ct} is a direct measure of corrosion [29,30], it could be stated that the corrosion of the hybrid composites in 0.1 M NaCl became more difficult in comparison to copper, which could be the result of strong molecular bonding among copper and reinforcing materials. Furthermore, CPE values of hybrid composites were slightly higher than that of cast copper, which could belong to presence of small size pits on the electrode surface. These pits were generated during manufacturing or corrosion process. The increase in n values for hybrid composites could be linked with the improved current distribution on the surface and

Table 4
Polarization curves data for cast cu, A1, A2 and A4 in 0.1 M NaCl.

Materials	-E_{corr} (V vs Ag/Agcl)	I_{corr} (μA cm^{-2})
Cu	0.072 ± 0.006	27.54 ± 2.62
A1	0.106 ± 0.008	7.76 ± 0.69
A2	0.085 ± 0.002	3.80 ± 0.23
A4	0.089 ± 0.003	1.52 ± 0.17

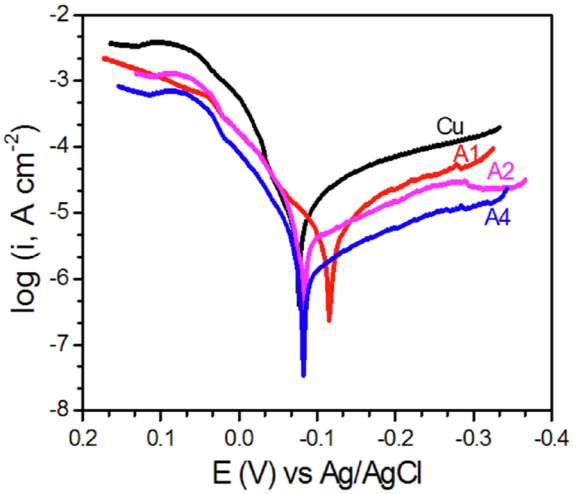

Fig. 14. Tafel plots of polarization curves for Cu, A1, A2 and A4.

supported by increase in phase angles (Fig. 13b). The W values decreased with HSSS concentration in copper matrix and thus indicated higher diffusion resistance of hybrid composites than copper. This fact could also suggest that diffusion of chloride to the metal surface, or transportation of metal-chloride complexes to NaCl solution, was significantly reduced in case of hybrid composites. The low χ^2 values suggested that discussion of corrosion behavior based on proposed AEC could be trusted with high confidence.

To know dynamic corrosion behavior of copper and composites, polarization curves are recorded and presented in Fig. 14. Analysis of Fig. 14 projected that polarization behaviors of Cu, A1, A2 and A4 in 0.1 M NaCl were similar in nature. However, the curves also suggested that downfalls of cathodic Tafel curves were more than anodic Tafel curves. This fact meant that the reinforcement in copper matrix retarded the reduction of active species on the surface more actively than metal dissolution, which was also evidenced by E_{corr} values (Table 5). However, the metal dissolution was also significantly reduced for the composites in comparison to cast copper. Further analysis of Fig. 14 revealed that both cathodic and anodic polarization curves shifted downward, which indicated lesser current generation in hybrid composites [31,32]. The low quantity of current could represent slow rate of corrosion reactions and symbolize retarded corrosion damage. The I_{corr} values for copper and composites confirmed the above mentioned fact (Table 5). It is a well known fact that corrosion current is a direct measure of corrosion rate [33,34]. Hence, it could be said that hybrid composites were more corrosion resistant than copper in 0.1 M NaCl. Another reason of lower I_{corr} values for the composites could be given based on relative activity of the A1, A2, A3 and Cu. As per galvanic series WC and HSSS are nobler to copper, meaning that polarizations of composites are more difficult in comparison to copper.

To further analyze the dynamic current response of the electrodes with potential, the linear currents of the copper and composites were plotted against applied potential (Inset of Fig. 15a). The power generated due to current responses have been calculated by the area of the current–potential curves and are shown in Fig. 15 along with i_{total} (total current = i_{anodic} + $i_{cathodic}$) values. A decrease in total current values could be observed while moving from copper to composites. This decrease could portray that rate of cathodic and anodic corrosion reactions lowered with the increase in HSSS concentration in the composites. In a similar way, reduction in power generation was acknowledged for the composites, which could correspond to less heat generation and could indicate lesser corrosion (current) of the composites than copper in 0.1 M NaCl. So, the ranking of the materials based on polarization responses of the copper and composites could be given as: A4 > A2 > A1 > Cu, which followed the results of EIS.

Conclusion

In this work, copper based hybrid composites were developed and examined by microstructure analysis, SEM, EDAX and XRD techniques. The mechanical testing of the composites suggested that composites were having higher hardness and ultimate tensile strength than cast copper. EIS results and Tafel polarization curves provided the fact that corrosion resistances of the hybrid composites were significantly greater than copper. The ranking of materials could be done based on hardness, UTS and corrosion resistance as: A4 > A2 > A1 > Cu. Thus, it was proposed based on this work that improvement in hardness and UTS as well as corrosion resistance of the composites could be mainly attributed to HSSS reinforcement in the copper matrix.

Acknowledgements

The authors are grateful to Professor Rajiv Prakash (in charge of CIFC, IIT BHU Varanasi) for providing surface characterization facilities.

Declaration of Competing Interest

Authors declare no conflict of interests.

Table 5
Impedance parameters obtained by fitting of Nyquist plots of cast cu, A1, A2 and A4 in 0.1 M NaCl.

Materials	R_s (Ω cm^2)	Rct (Ω cm^2)	CPE (μS.sec^n cm^{-2})	n	W (μS.$sec^{0.5}$)	χ^2 (10^{-4})
Cu	36 ± 7	1636 ± 25	21.6 ± 1.8	0.609 ± 0.001	2634 ± 23	75.5
A1	73 ± 5	2809 ± 39	30.8 ± 2.3	0.610 ± 0.002	1718 ± 33	30.7
A2	58 ± 2	3970 ± 53	29.7 ± 2.1	0.615 ± 0.001	1700 ± 27	40.7
A4	55 ± 6	5092 ± 67	57.0 ± 1.6	0.751 ± 0.004	0504 ± 13	9.74

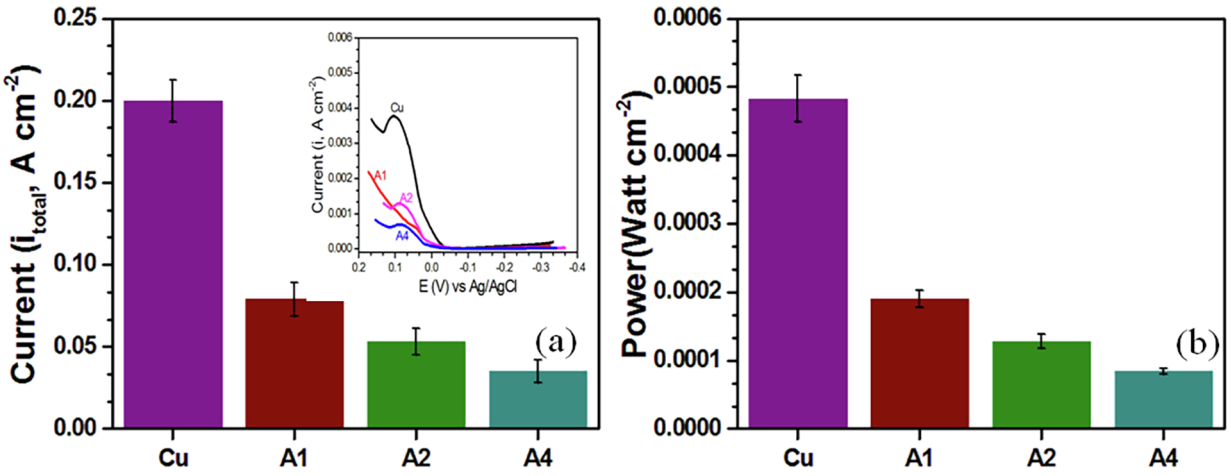

Fig. 15. Total current (i_{total}) for Cu, A1, A2 and A4.

Appendix A. Supplementary data

Supplementary data to this article can be found online at https://doi.org/10.1016/j.rinp.2019.102319.

References

[1] Mallik S, Ekere N, Best C, Bhatti R. Investigation of thermal management materials for automotive electronic control units. Appl Therm Eng 2011;31:355–62.

[2] Molina A, Wang T, Zou C, Chen Z, Li M, Wang W, et al. In situ synthesis of TiB2 particulate reinforced copper matrix composite with a rotating magnetic field. Mater Des 2015;65:280–8.

[3] Kumari S, Kumar A, Sengupta PR, Dutta PK, Mathur RB. Improving the mechanical and thermal properties of semi-coke based carbon/copper composites reinforced using carbon nanotubes. J Adv Mater Lett 2014;5:265–71.

[4] Zitoune R, El Mansori M, Vijayan K. Tribo-functional design of double cone drill implications in tool wear during drilling of copper mesh/CFRP/woven ply. Wear 2013;302:1560–7.

[5] Yusoff M, Othman R, Hussain Z. Mechanical alloying and sintering of nanostructured tungsten carbide-reinforced copper composite and its characterization. Mater Des 2011;32:3293–8.

[6] Thakre AA, Soni S. Modeling of burr size in drilling of aluminum silicon carbide composites using response surface methodology. Eng Sci Technol 2016;19:1199–205.

[7] Gautam RK, Ray S, Sharma SC, Jain SC, Tyagi R. Dry sliding wear behavior of hot forged and annealed Cu–Cr–graphite in-situ composites. Wear 2011;271:659–64.

[8] Moustafa SF, Abdel-Hamid Z, Abd-Elahi AM. Copper matrix SiC and Al2O3 particulate composites by powder metallurgy technique. Mater Lett 2002;53:244–9.

[9] Grünberger W, Heilmaier M, Schultz L. High-strength, high-nitrogen stainless steel–copper composite wires for conductors in pulsed high-field magnets. Mater Lett 2002;52(3):154–8.

[10] Bakkar A, Ataya S. Corrosion behaviour of stainless steel fibre-reinforced copper metal matrix composite with reference to electrochemical response of its constituents. Corros Sci 2014;85:343–51.

[11] Hamada AS, Khosravifard A, Kisko AP, Ahmed EA, Porter DA. High temperature deformation behavior of a stainless steel fiber-reinforced copper matrix composite. Mater Sci Eng, A 2016;669:469–79.

[12] Xavior A, Kumar A. Machinability of hybrid metal matrix composite – a review. Procedia Eng 2017;174:1110–8.

[13] Ramesh CS, Noor Ahmed R, Mujeebu MA, Abdullah MZ. Development and performance analysis of novel cast copper-SiC–Gr hybrid composites. Mater Des 2009;30:1957–65.

[14] Kovalchenko AM, Fushchich OI, Danyluk S. The tribological properties and mechanism of wear of Cu-based sintered powder materials containing molybdenum disulfide and molybdenum diselenite under unlubricated sliding against copper. Wear 2012;290–291:106–23.

[15] Ramesh CS, Noor Ahmed R, Mujeebu MA, Abdullah MZ. Fabrication and study on tribological characteristics of cast copper–TiO_2–boric acid hybrid composites. Mater Des 2009;30:1632–7.

[16] Vamsi Krishna M, Xavior Anthony M. An investigation on the mechanical properties of hybrid metal matrix composites. Procedia Eng. 2014;97:918–24.

[17] Subramanya Reddy P, Kesavan R, Vijaya Ramnath B. Investigation of mechanical properties of aluminium 6061-silicon carbide, boron carbide metal matrix composite. Silicon 2018;10:495–502.

[18] Samal CP, Parihar JS, Chaira D. The effect of milling and sintering techniques on mechanical properties of Cu–graphite metal matrix composite prepared by powder metallurgy route. J Alloys Compd 2013;569:95–101.

[19] Singh MK, Gautam RK. Synthesis of copper metal matrix hybrid composites using stir casting technique and its mechanical, optical and electrical behaviours. Trans Indian Inst Met 2017;70:2415–28.

[20] Bagheri GHA. The effect of reinforcement percentages on properties of copper matrix composites reinforced with TiC particles. J Alloys Compd 2016;676:120–6.

[21] Alaneme K, Odoni B. Mechanical properties, wear and corrosion behavior of copper matrix composites reinforced with steel machining chips. Eng Sci Technol Int J 2016;19:1593–9.

[22] Li J, Zhang H, Zhang Y, Che Z, Wang X. Microstructure and thermal conductivity of Cu/diamond composites with Ti-coated diamond particles produced by gas pressure infiltration. J Alloys Compd 2015;647:941–6.

[23] Ares AE, Gassa LM. Corrosion susceptibility of Zn–Al alloys with different grains and dendritic microstructures in NaCl solutions. Corros Sci 2012;59:290–306.

[24] Rosalbino F, Angelini E, Macciò D, Saccone A, Delfino S. Application of EIS to assess the effect of rare earths small addition on the corrosion behavior of Zn–5% Al (Galfan) alloy in neutral aerated sodium chloride solution. Electrochim Acta 2009;54:1204–9.

[25] Ji G, Dwivedi P, Sundaram S, Prakash R. Aqueous extract of Argemone mexicana roots for effective protection of mild steel in an HCl environment. Res Chem Intermed 2016;42:439–59.

[26] Srivastava M, Tiwari P, Kumar A, Ji G, Prakash R. Low cost aqueous extract of pisum sativum peels for inhibition of mild steel corrosion in 1 M HCl. J Mol Liq 2018;254:357–68.

[27] Ji G, Macia LF, Allaert B, Hubin A, Terryn H. Odd random phase electrochemical impedance spectroscopy to study the corrosion behavior of hot dip Zn and Zn-alloy coated steel wires in sodium chloride solution. J Electrochem Soc 2018;165:C246–57.

[28] Abdel-Aal MS, Ahmed ZA, Hassan MS. Inhibiting and accelerating effects of some quinolines on the corrosion of zinc and some binary zinc alloys in HCl solution. J Appl Electrochem 1992;22:1104–9.

[29] Srivastava M, Tiwari P, Srivastava SK, Prakash Rajiv, Ji G. Electrochemical investigation of Irbesartan drug molecules as an inhibitor of mild steel corrosion in 1 M HCl and 0.5 M H_2SO_4 solutions. J Mol Liq 2017;236:184–97.

[30] Curioni M, Scenini F, Monetta T, Bellucci F. Correlation between electrochemical impedance measurements and corrosion rate of magnesium investigated by real-time hydrogen measurement and optical imaging. Electrochim Acta 2015;166:372–84.

[31] Ji G, Anjum S, Sundaram S, Prakash R. Musa paradisica peel extract as green corrosion inhibitor for mild steel in HCl solution. Corros Sci 2015;90:107–17.

[32] Yadav DK, Chauhan DS, Ahamad I, Quireshi MA. Electrochemical behavior of steel/acid interface: adsorption and inhibition effect of oligomeric aniline. RSC Adv 2013;3:632–46.

[33] Ji G, Dwivedi P, Sundaram S, Prakash R. Inhibitive effect of Chlorophytum borivilianum root extract on mild steel corrosion in HCl and H_2SO_4 solutions. Ind Eng Chem Res 2013;52:10673–81.

[34] Dean SW, France Jr. WD, Ketcham SJ. Electrochemical methods. In: Ailor WH, editor. Handbook on Corrosion Testing and Evaluation. New York: John Wiley; 1971. p. 173–4.